Acta Pharmaceutica Sinica B 2024;14(12):5201−5218

Chinese Pharmaceutical Association
Institute of Materia Medica, Chinese Academy of Medical Sciences

Acta Pharmaceutica Sinica B

www.elsevier.com/locate/apsb
www.sciencedirect.com

ORIGINAL ARTICLE

UBE2G2 inhibits vasculogenic mimicry and metastasis of uveal melanoma by promoting ubiquitination of LGALS3BP

Andi Zhao[a,b], Chenyu Zhou[a,b], Jinjing Li[a,b], Zijin Wang[a], Hui Zhu[a], Shiya Shen[a], Qing Shao[a], Qi Gong[a], Hu Liu[a,b,*], Xuejuan Chen[a,b,*]

[a]*Department of Ophthalmology, the First Affiliated Hospital with Nanjing Medical University, Nanjing 210029, China*
[b]*Nanjing Medical University, Nanjing 211166, China*

Received 22 April 2024; received in revised form 19 June 2024; accepted 26 July 2024

KEY WORDS

UBE2G2;
Vasculogenic mimicry;
Invasion and metastasis;
Uveal melanoma;
Ubiquitination;
Tumor microenvironment;
LGALS3BP;
Hypoxia

Abstract Uveal melanoma (UM) poses a significant lethality, with approximately 50% of those developing metastases surviving less than one year. In the progression of UM, vasculogenic mimicry (VM) induced by hypoxia plays a pivotal role, which also partially explains the resistance of UM to anti-angiogenic therapies. Nevertheless, the crucial molecular mechanisms underlying VM in the progression of UM remain unclear. We identified ubiquitin conjugating enzyme E2 G2 (UBE2G2) as a critical suppressor through transcriptomic sequencing and metastasis correlation screening. In UM, hypoxia-induced VM and metastasis are markedly exacerbated by UBE2G2 knockdown and significantly alleviated by its overexpression. Mechanistically, UBE2G2 directly binds to galectin 3 binding protein (LGALS3BP) and forms a complex with the E3 ubiquitin ligase tripartite motif containing 38 (TRIM38), facilitating ubiquitination-mediated degradation of LGALS3BP at the K104 residue. Furthermore, UBE2G2 inhibits oncogenic phenotypes by inactivating intracellular PI3K/AKT signaling and reprogramming the tumor microenvironment. Therefore, targeting intercellular and intracellular molecular mechanisms of the hypoxia−UBE2G2−LGALS3BP axis may contribute to developing various therapeutic strategies for UM.

*Corresponding authors.
E-mail addresses: liuhu@njmu.edu.cn (Hu Liu), xuejuanchen1866@njmu.edu.cn (Xuejuan Chen).

Peer review under the responsibility of Chinese Pharmaceutical Association and Institute of Materia Medica, Chinese Academy of Medical Sciences.

https://doi.org/10.1016/j.apsb.2024.09.005

1. Introduction

Uveal melanoma (UM) is the most common primary intraocular malignancy in adults[1]. Although enucleation or plaque radiotherapy can control the primary eye tumor, about half of the patients still develop metastases[2]. Once distant metastasis has occurred, the mean survival time of patients drops to less than one year[3]. Therefore, comprehending the mechanisms of metastasis in uveal melanoma is a crucial step towards enhancing the outcomes.

Recent studies have shown that vasculogenic mimicry (VM) is emerging as a critical factor in metastasis[4–6]. Due to the imbalance between abnormal vascularization and hypoxic microenvironment, tumor cells induce the formation of vascular-like structures to facilitate the supply of nutrients and oxygen delivery. This phenomenon, initially reported by Maniotis et al.[7] in 1999, is called VM. The occurrence of VM correlates with a higher tumor grade, shorter survival, increased invasion, and metastasis. Formed by plastic tumor cells independently mimicking vascular endothelial cells, VM represents a distinct pattern of tumor neovascularization without endothelial cell participation. Given the presence of VM, the efficacy of anti-angiogenic agents is limited in controlling the progression of UM[8]. Therefore, unraveling the mechanistic link behind VM holds the potential to enhance the current landscape of UM treatment and long-term prognosis.

A hypoxic environment is commonly recognized as the most potent inducer of VM, a phenomenon frequently observed in the microenvironment of solid tumors, including uveal melanoma. In UM, our understanding of the impact of hypoxia on tumor progression remains limited despite some previous investigations[9–11]. Furthermore, previous research primarily focused on stabilizing the hypoxia inducible factor 1 subunit alpha (HIF1α) family and its role as a transcription factor regulating the expression of downstream target genes. Nevertheless, it is worth noting that protein destabilization through hypoxia-regulated ubiquitination has also been documented[12–14].

Ubiquitination, a post-translational modification process, is pivotal in mediating protein degradation in eukaryotic cells[15]. This highly dynamic and reversible mechanism is mediated by the ubiquitin-proteasome system (UPS), including E1 ubiquitin-activating enzymes, E2 ubiquitin-conjugating enzymes, and E3 ubiquitin ligases[16]. Accumulated evidence suggests that the dysfunction of the UPS is implicated in multiple aspects of tumor progression, including cell proliferation, migration, invasion, and metastasis[17–19]. Recent studies also indicated the potential of the UPS in developing novel regimens for UM[17]. However, there is a deficiency of studies on hypoxia that facilitate vasculogenic mimicry and promote tumor cell invasiveness through ubiquitin signaling.

This study explores the role of the UPS in hypoxia-induced VM and metastasis in UM. Our findings indicate that ubiquitin-conjugating enzyme E2 G2 (UBE2G2) expression inhibits VM and metastasis, accompanied by a decreased desmoplastic response. Targeting intercellular and intracellular aspects of the hypoxia−UBE2G2−galectin 3 binding protein (LGALS3BP) axis may inform diverse therapeutic strategies for UM.

2. Materials and methods

2.1. Human specimens and cell lines

A total of 7 ocular melanoma tissues and 7 human normal melanocyte tissues were acquired with signed informed consent from First Affiliated Hospital of Nanjing Medical University. Fresh specimens were immediately stored at −80 °C until use. The study was approved by the Human Ethics Committee of the Hospital (Approval number: 2022-SRFA-334), and each patient signed informed consent before the research started. The clinicopathological characteristics are provided in Supporting Information Table S1.

Human UM cell lines (Mel270, MUM2B, Omm2.5), as well as human embryonic kidney cell line (HEK293T), and the mouse melanoma cell line (B16F10) were purchased from the Cell Bank of Type Culture Collection of the Chinese Academy of Sciences (Shanghai, China). Cells were cultured under previously described conditions at 37 °C in a humidified atmosphere with 5% CO_2[20]. For hypoxia experiments, cells were placed in an anaerobic bag with an oxygen indicator (AnaeroPack™, Mitsubishi gas chemical, Japan).

2.2. Cell transfection

Recombinant lentiviruses carrying the full-length sequence, short hairpin RNAs (shRNAs) and related negative control were synthesized by Obio (China).

A series of mutant plasmids of UBE2G2, LGALS3BP, and ubiquitin were synthesized by Obio. According to the manufacturer's instructions, Lipofectamine 3000 (Invitrogen, USA) was utilized to transfer shRNAs and plasmid vectors into the cells. The infection's effectiveness was verified through real-time quantitative reverse transcription polymerase chain reaction (qRT-PCR) and western blotting.

2.3. Quantitative real-time PCR

RNA samples from this study's UM tissue specimens and cell lines were extracted with TRIzol reagent (Invitrogen, USA). Total RNA was reversely transcribed to cDNA using HiScript RT Mix (Vazyme, China). Relative RNA levels determined by qRT-PCR were measured using the SYBR Green PCR kit (Vazyme, China) on a Q7 Real-Time PCR System (Applied Biosystems, USA). The relative levels of RNA were calculated using the comparative CT ($2^{-\Delta\Delta CT}$) method, and β-actin was employed as an internal control. Primers used for this analysis are listed in Supporting Information Table S2.

2.4. Western blotting

Proteins were extracted from UM tissues and cells using RIPA lysis buffer (Beyotime, China) containing protease inhibitors (Beyotime, China). The proteins were resolved by electrophoresis in SDS-PAGE gels, transferred to PVDF membranes (0.45 mm, Solarbio, China), and blocked in a blocking buffer (Beyotime, China) for 30 min. The PVDF membranes were incubated with primary antibodies overnight at 4 °C, and an anti-β-actin monoclonal antibody was used as loading controls and normalization. Afterwards, at room temperature, immune blotting was conducted using HRP-conjugated secondary antibodies for 2 h. Finally, the protein bands were detected by chemiluminescence using an electrochemiluminescence system (YEASEN, China). The antibodies used in this assay are listed in Supporting Information Table S3.

2.5. Wound healing and transwell assays

Wound healing and transwell assays were performed to evaluate cell migration and invasion abilities. For wound-healing assays,

the transfected UM cells were cultured in a 6-well plate until confluence, and a linear wound was scraped with a 200-mL pipette tip. The plate was imaged at the same position, the gap distance was evaluated at 0 h ($s1$) and 24 h ($s2$), and the Migration ability (%) was calculated as Eq. (1):

$$\text{Migration ability (\%)} = (s1-s2)/s1\times 100 \quad (1)$$

For Transwell assays, 200 mL of serum-free medium containing 2×10^4 transfected cells were seeded in the upper chamber of a Transwell plate (Corning, USA), and 800 mL of serum-containing medium was added to the lower part of the Transwell unit. After 24 h of incubation, the cells in the upper chamber were fixed, stained with crystal violet (Beyotime, China) for 20 min, and observed using an inverted optical microscope (Olympus, Japan). Three fields of view were randomly selected for cell counting. Matrigel (BD Biosciences, USA) was pre-coated onto the plate surface for the invasion assay to explore the invasive ability of the cells.

2.6. *In vitro vascular mimicry assay*

The 96-well plate wells were covered with 50 μL of ice-cold growth factor-reduced Matrigel (Corning, USA), and plates were placed in a cell incubator at 37 °C for 30 min MUM2B cells (1×10^4 cells per well), Mel270 cells (1.5×10^4 cells per well), or Omm2.5 cells (1.5×10^4 cells per well) were seeded on Matrigel. All cells were incubated under normoxia for 1 h before incubating in normoxia or hypoxia conditions for 24 h. Tube formation of vascular mimicry was visualized under an Olympus light microscope (10 objective magnification).

2.7. *RNA sequencing*

MUM2B cells were treated with normoxia (21% O_2) and hypoxia (1% O_2) for 24 h, respectively, and total RNA was extracted using TRIzol reagent (Beyotime, China). The integrity of the RNA was verified using the Agilent 2100 Bioanalyzer (Genesky, China). Next, mRNA was purified and fragmented to lengths between 100 and 300 bp using Oligo-dT magnetic beads. The synthesis of both the first and second strands of cDNA followed this—subsequent steps involved end repair, adenylating the 3′ ends and ligating adapters. After selecting fragment sizes and amplifying them *via* PCR, the HiSeq system by Illumina, carried out high-throughput RNA sequencing in Pair End mode. To identify differentially expressed genes (DEGs) between the two sample groups, we utilized the Deseq2 package in R (version 3.6.3). DEGs were pinpointed using a threshold of an absolute fold change (FC) value ($|\log2FC| > 2$ and a P-value <0.01.

2.8. *Co-immunoprecipitation (Co-IP) assay with label-free proteomics analysis*

Co-IP assays were performed to validate the physical interactions with the target protein with the IP/Co-IP Kit (Thermo Fisher Scientific, USA). Cells were lysed with lysis buffer; lysates were incubated with a specific antibody at 4 °C overnight. The immune complex was incubated with A/G-agarose beads for 1 h at room temperature, and then magnetic beads were washed twice with lysis buffer to remove non-specifically bound proteins. The products dissolved in 1 × SDS lysis buffer, denatured at 95 °C for 10 min, and finally run on a gel to separate by size. Western blot or mass spectrometry (Biotree, China) was used to detect or visualize the immunoprecipitated protein.

Label-free proteomics analysis was used to analyze the protein abundance between UBE2G2-overexpressing and control groups. A Student's t-test identified significant differences. Peptides that met the following criteria were considered to be differentially expressed: FC $\geq$ 1.2 or FC $\leq$ 0.83 and P-value <0.05.

2.9. *Glutathione S-transferase (GST)-fusion pull-down assay*

FLAG-tagged UBE2G2 expression plasmids were transfected into *E. coli*, purified using a Ni^{2+}-NTA-chelating column (Thermo Fisher Scientific, USA). GST-fusion assays were performed according to the manufacturer's instructions. Briefly, 50 mg of GST-LGALS3BP or GST was Equilibrate glutathione Sepharose beads (Sigma, USA) and incubated with 20 mg of purified Flag-UBE2G2. Following overnight incubation, unbound proteins were eliminated, while bound proteins were extracted from the beads with SDS sample buffer. The bound proteins were separated through SDS-PAGE gel and pinpointed with Western blotting using anti-FLAG and GST antibodies.

2.10. *Ubiquitination assay*

Cells were transfected with indicated plasmids or shRNAs, treated with proteasome inhibitor MG132 (Beyotime, China) for 6 h and then lysed to extract proteins. The anti-Myc antibody was used to perform immunoprecipitation to isolate the protein and its modified forms. After washing, elution, neutralization, and boiling, the status of protein ubiquitination was analyzed by immunoblotting with an antibody against ubiquitin.

2.11. *Animal studies*

As previously described[11], twelve-week-old female C57BL/6 (10 mice/group) or BALB/c nude mice (10 mice/group) were used for the suprachoroidal tumor formation and liver and lung metastasis model. All experiments were under IACUC approval and adherence to the institutional guidelines of the Committee on the Ethics of Animal Experiments of Nanjing Medical University (Approval number: IACUC-2303037). On Day 0, transfected melanoma cells (1×10^6 cells/100 μL) were inoculated into the suprachoroidal space of the right murine eye using a *trans*-scleral technique. The eyes with tumors were removed on the 7th (B16F10) or 9th day (MUM2B) after inoculation, and livers with metastases were collected at the time of sacrifice 4 (B16F10) to 8 weeks (MUM2B) after injection. In the Kaplan−Meier survival experiments, the mice were kept alive until they met the IACUC criteria for termination (usually >20% of body weight loss) after undergoing enucleation. Eyes, livers, and lung tissues were surgically removed, fixed, and assessed using hematoxylin staining.

2.12. *Histological analyses*

For immunohistology analysis, tumor tissues were fixed with 4% paraformaldehyde, embedded in paraffin, cut into 5 μm-thick-sections, and then deparaffinized, followed by hematoxylin and eosin staining according to standard procedures.

For the immunofluorescent assay, tissue samples were embedded in the optimal cutting temperature compound and sliced into 10-μm-thick frozen sections. The tissue sections were

permeabilized using 0.3% Triton X-100, blocked with 1% BSA at room temperature and then incubated with primary antibodies at 4 °C overnight. After washing three times with PBS, each specimen was incubated with a secondary antibody labeled with a fluorescent dye. The cell nuclei were stained with DAPI (Beyotime, China) for 5 min at room temperature. Finally, the stained cells and tissues were observed and imaged using a fluorescent microscope (Thunder Image, LEICA, Germany).

2.13. Statistical analysis

The statistical analyses and graphing were performed using Graph-Pad Prism 8.0 (GraphPad, USA). Differences between two groups were calculated using Student's *t*-test and three or more groups using one-way ANOVA. For the survival studies, the Kaplan−Meier method and the log-rank test were applied for statistical comparisons in survival distributions. The expression levels of various genes were correlated using Spearman's rank correlation test. Differences were considered significant for P values < 0.05.

3. Results

3.1. UBE2G2 is significantly downregulated in UM and correlated with advanced clinicopathological features and poor prognosis

To validate whether hypoxia promotes the malignant phenotypes of UM cells, transwell and vascular mimicry assays were performed under both normoxic (21% O_2) and hypoxic (1% O_2) conditions based on previous literature[9,21,22]. The Western blot assay measured the expression of HIF1α under the hypoxic condition at 0, 6, 12, and 24 h (Supporting Information Fig. S1A). Results showed that hypoxia promotes migration (Fig. S1B) and tube formation (Fig. 1A) of UM cell lines. Subsequently, we conducted RNA sequencing to identify the differently expressed genes between normoxic and hypoxia conditions for 24 h in MUM2B (Fig. 1B). To gain an insight as to which ones might underlie UM development, we screened genes expressed differentially both in RNA sequence ($|\log2FC| > 2$, P value < 0.01) and in a publicly available database of primary melanoma patients who either developed metastasis or did not [GSE27831 ($|\log2FC| > 1$, P value < 0.05)]. Then, outcome analysis using the iUUCD 2.0 database evidenced that the gene expression of 5 of these was correlated with ubiquitination, which was summarized in a Venn diagram (Fig. 1C). Among them, expression differences of 4 genes (*CASS4*, *NEDD9*, *TRIM59* and *UBE2G2*) in GSE27831 were consistent with the change trends in hypoxia (Fig. 1D and Fig. S1C). Since qRT-PCR and Western blot demonstrated that UBE2G2 downregulated consistently and most dramatically by hypoxia in 4 UM cell lines, it was chosen for subsequent research (Fig. 1E and F). UBE2G2 protein expression was remarkably lower in the Omm2.5 cell line (originating from metastatic lesions) compared with the Mel270 cell line (generated from primary uveal melanoma tumors) (Fig. 1F)[23]. Re-analyzing a recently published single-cell dataset, the distribution indicated UBE2G2 was generally lowly expressed in UM (Fig. S1D). Consistently, UM tissues had lower UBE2G2 protein levels than normal tissues in our samples (Fig. 1G). Kaplan−Meier analyses on two datasets (GSE22138 and GSE27831) showed that decreased mRNA expression of *UBE2G2* strongly correlates with patient distant metastasis-free survival (Fig. 1H). Furthermore, immunofluorescent staining confirmed that the hypoxic region, labelled with a hypoxia probe pimonidazole (green), was correlated with the lower expression levels of UBE2G2, especially in samples collected from UM patients compared with health controls (Fig. 1I). These results show that UBE2G2 expression was a valuable marker for predicting UM metastatic progression and prognostic for patient outcome. They also suggest that UBE2G2 may play an essential role in the metastatic process in UM.

3.2. UBE2G2 inhibits UM cell metastasis and tube formation especially in hypoxia

We performed a series of cell functional assays to assess whether UBE2G2 could modulate metastasis and tube formation ability of UM cells caused by hypoxia. According to our detection of UBE2G2 expression across four UM cell lines, we utilized lentivirus-mediated infection to knock down UBE2G2 in MUM2B, Mel270, and B16F10 while overexpressing it in MUM2B, Omm2.5, and B16F10. The transfection efficiency of the four cell lines was assessed *via* qRT-PCR and Western blot assay. Sh-UBE2G2#3 demonstrated the highest knockdown efficiency across all cell lines and was used for further experiments (Fig. S1E and S1F).

Next, we utilized the transwell and scratch wound healing assays to evaluate cell migration and invasion capability. UBE2G2 knockdown prominently promoted the invasion and migration ability of Mel270 and MUM2B cells, especially in hypoxic conditions. In contrast, overexpressed UBE2G2 suppressed this ability in Omm2.5 and MUM2B cells, notably under hypoxia (Fig. 2A−D, Supporting Information Fig. S2A−S2D). Furthermore, the vascular mimicry assay to measure the VM formation ability of UM cells. After suppressed UBE2G2 expression, the overall morphology of the tube network appeared more regular and presented a better tube structure, whereas UBE2G2 overexpression abated this ability in hypoxia. These changes were quantitatively reflected in total branching points (Fig. 2E and F, Fig. S2E and S2F). Similarly, the expression of VE-cadherin, a master gene of vasculogenic mimicry, also reveals an improvement in MUM2B and Mel270 after UBE2G2 decreased, while a visible reduction in Omm2.5 and MUM2B with upregulated UBE2G2 (Fig. 2G and H, Fig. S2G and S2H). These results show that hypoxia enhances UM cell migration, invasion and VM ability at least in part through UBE2G2 reduction, while overexpressed UBE2G2 can potently antagonize this response.

Then, we investigated whether UBE2G2 affects primary and metastatic UM growth *in vivo*. Two complementary orthotopic UM models in mice were established to mimic the human UM disease process. The first entailed injecting mouse melanoma cells (B16F10) into the immunocompetent syngeneic C57BL/6 mice. In the second model, human UM cells (MUM2B) were injected into the immunodeficient BALB/c nude mice (Fig. 3A). The injection of UBE2G2 knockdown and overexpression cells into the subuveal area of the mouse eye can lead to the formation of melanomas, which can then spontaneously metastasize to the liver and lung. UBE2G2 and LGALS3BP (downstream of UBE2G2) protein levels were verified by immunofluorescence analysis of eye tumor sections (Fig. 3B; Supporting Information Fig. S3A). Both models showed that cells with depleted UBE2G2 had a promoting eye tumor formation, reflected in more tumor weight than control 7 or 9 days post-inoculation, while overexpression of UBE2G2 exhibited an opposite effect (Fig. 3C and D, Fig. S3B and S3C).

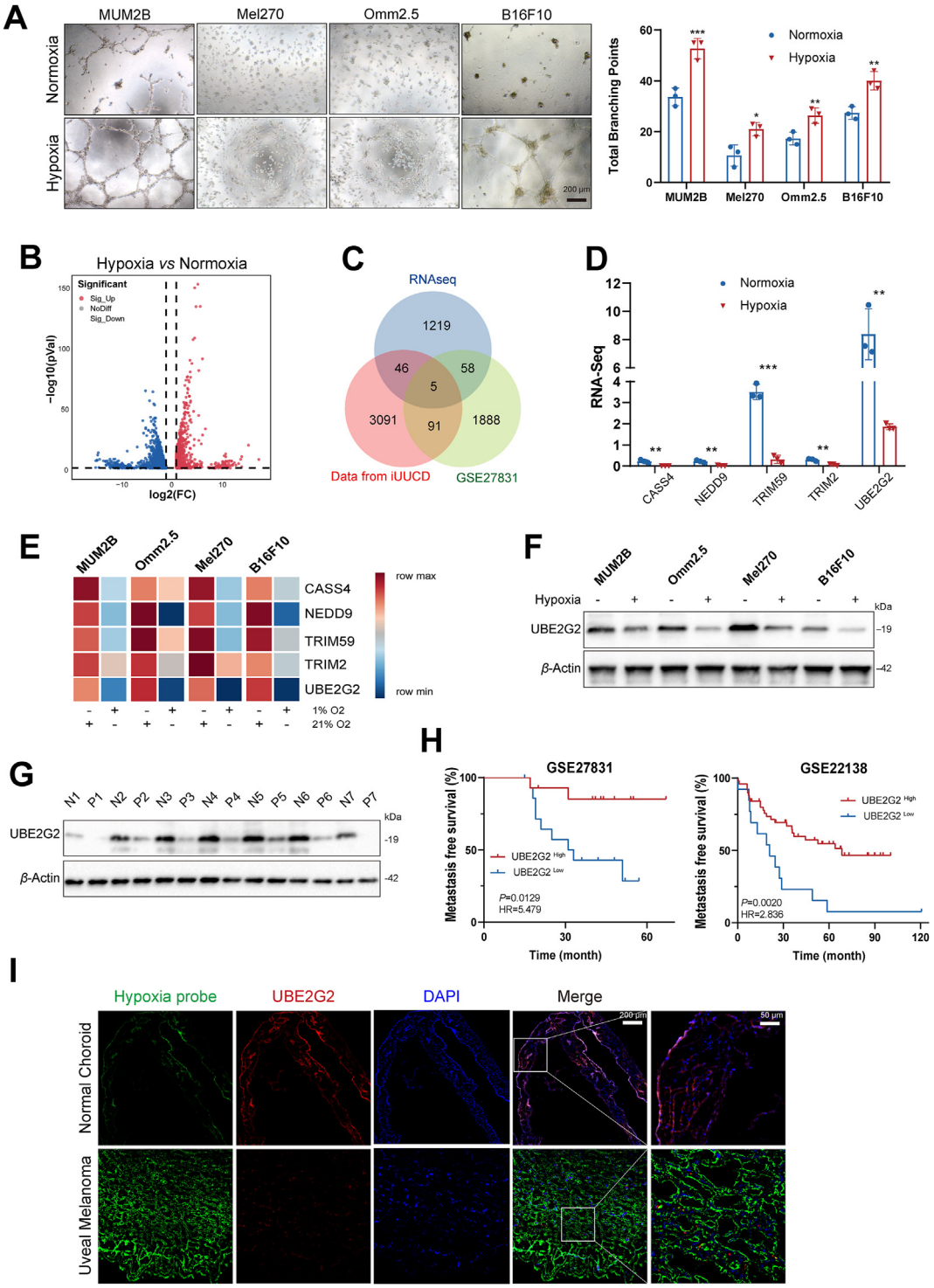

Figure 1 UBE2G2 is downregulated by hypoxia in uveal melanoma (UM) and correlated with metastasis. (A) Four melanoma cell lines (MUM2B, Mel270, Omm2.5, B16F10) were cultured on Matrigel under normoxia or hypoxia for 24 h (Left). Branching points of tube formation were quantified (Right). (B) Volcano plot showing the transcriptome data of MUM2B cultured under hypoxia for 24 h. (C) Venn diagram showing the number of overlapping genes. (D) RNA-Seq quantified the relative expression of five identified genes. (E) Heatmap of qRT-PCR data probing expression of five identified genes in melanoma cell lines under hypoxia. β-Actin was used as internal control, and results are expressed as fold change over normoxic control. Data are presented as relative expressions. (F) The protein level of UBE2G2 in five melanoma cell lines under normoxia or hypoxia for 24 h. (G) Protein level of UBE2G2 in seven UM tissues and normal uveal tissues. (H) Kaplan−Meier Metastasis-free survival curves of UM patients with high and low expression of UBE2G2 genes from GSE22138 and GSE27831 UM cohorts. (I) Representative images of the hypoxic region (hypoxia probe: pimonidazole staining) and UBE2G2 expression in UM tissues and normal control. All data are presented as the mean ± SD of three independent experiments. $^{*}P < 0.05$, $^{**}P < 0.01$, $^{***}P < 0.001$.

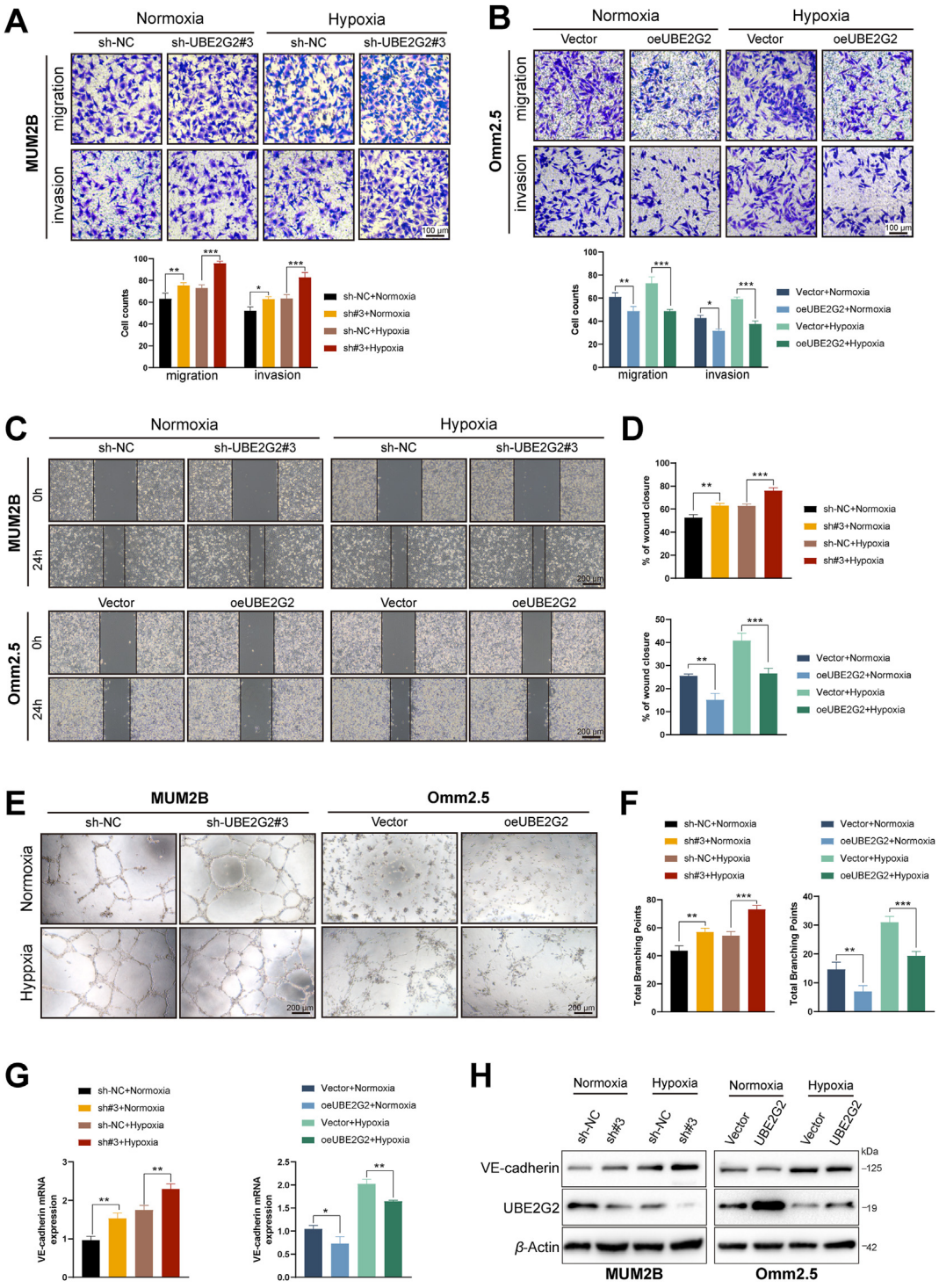

Figure 2 UBE2G2 inhibits UM cell metastasis and vasculogenic mimicry (VM) induced by hypoxia *in vitro*. (A, B) Transwell assays were performed to evaluate the migration and invasion abilities of UM cells. (C, D) Wound healing assays were used to assess cell migration ability. (E, F) Matrigel tube formation was performed to evaluate the vasculogenic mimicry abilities of UM cells. (G, H) The mRNA and protein level of VE-cadherin (a marker of VM) were used to assess cell vasculogenic mimicry ability. All data are presented as the mean ± SD of three independent experiments. $*P < 0.05$, $**P < 0.01$, $***P < 0.001$.

To further examine whether it could affect metastasis *in vivo*, we quantified micrometastases in liver and lung sections after mice reached IACUC criteria for termination (Fig. 3E and Fig. S3D and S3E). UBE2G2 silenced group showed a noticeable increase in hepatic as well as pulmonary metastatic foci, whereas a diminished number of hepatic as well as pulmonary metastatic nodules in the UBE2G2-overexpressed group (Fig. 3F and G, Fig. S3F and S3G). Based on a recent article, the presence of VM *in vivo* was determined through co-immunofluorescence staining using CD34 as an endothelial-specific marker, S100B as a

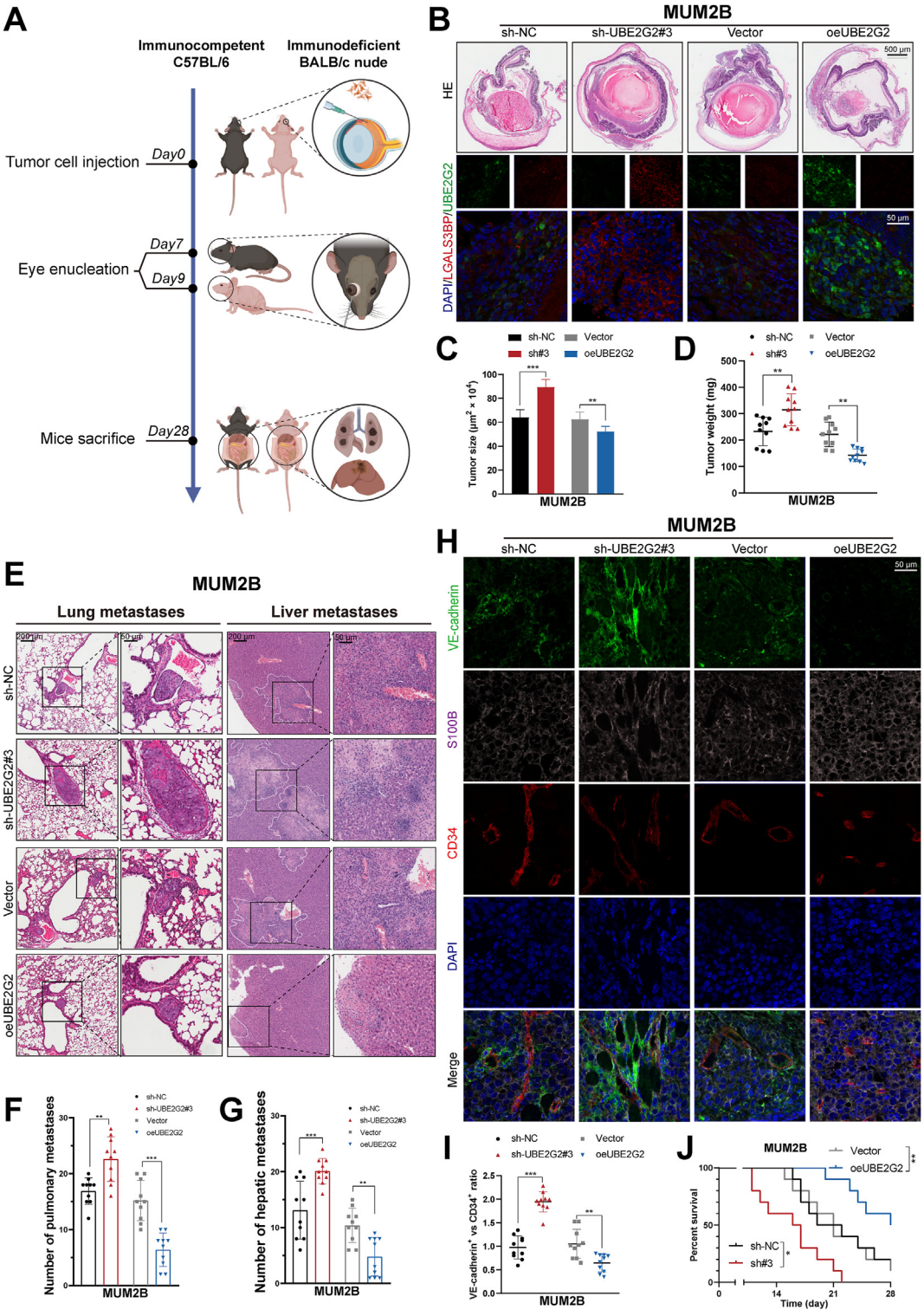

Figure 3 UBE2G2 inhibits UM cell metastasis and VM *in vivo*. (A) Schematic showing the timeline and procedure for the animal experiments. (B−D) MUM2B cells (1×10^6/eye) were injected in the sub-uveal area of BALB/c nude mice eyes, where they form melanomas in the uvea. On Day 9, tumor-bearing eyes were enucleated, fixed, and stained to evaluate tumor burden. Representative images of hematoxylin and eosin staining and co-immuno staining of tumor-bearing eyes (B), along with quantification of eye tumor size (C) and tumor weight (D). (E−G) Mice were sacrificed on Day 28, and hematoxylin and eosin stainings of liver and lung metastases were obtained from nude mice (E). The number of pulmonary metastasis (F) and hepatic metastasis (G). (H) MUM2B-derived tumor sections were co-immunostained for CD34, VE-cadherin, and S100B. VM channels: $CD34^-/VE^-cadherin^+/S100B^+$, endothelial vessels: $CD34^+/VE^-cadherin^+/S100B^-$. (I) Statistical analysis of VE-cadherin/CD34 expression ratio in UM orthotopic xenografts. (J) After eye enucleation, mice were euthanized when reaching the IACUC endpoint criteria. Kaplan−Meier analysis was used to measure the survival of mice burdened with metastatic melanoma. All data are presented as the mean ± SD of independent experiments. $^*P < 0.05$, $^{**}P < 0.01$, $^{***}P < 0.001$.

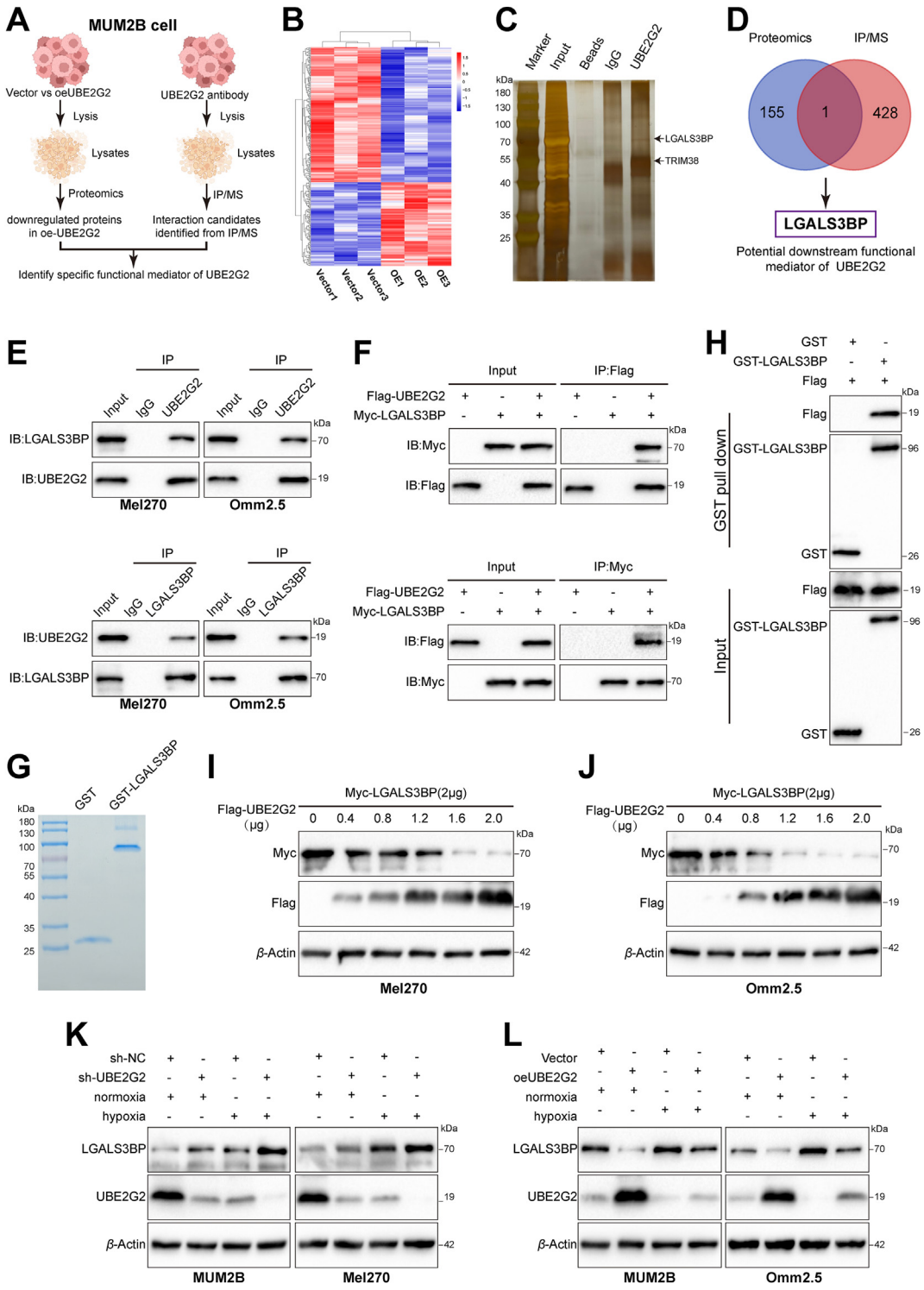

Figure 4 UBE2G2 interacts with galectin 3 binding protein (LGALS3BP) and negatively regulates its protein level. (A) Scheme displaying the procedure used for identifying the specific target of UBE2G2. (B) Heatmap showing dysregulated proteins (red, upregulated proteins; blue, downregulated proteins) identified by proteomics assays. $n = 3$ replicates per group. (C) Silver staining of UBE2G2 immunoprecipitation lysates. Arrows show different bands in co-immunoprecipitation (Co-IP) assays between the UBE2G2 group and IgG group. (D) The Venn diagram shows the intersection of the results from the proteomics and IP/MS analyses. (E) Mel270 and Omm2.5 cells were cultured under normoxia and then treated with MG132 (10 μmol/L) for 6 h before harvesting. Cell lysates were analyzed by Co-IP followed by Western blotting. (F) HEK293T cells transfected with indicated plasmids for 24 h were treated with MG132 (10 μmol/L) for 6 h. Co-IP and Western blotting assay detected the exogenous interaction between UBE2G2 and LGALS3BP. (G) glutathione *S*-transferase (GST) fusions of LGALS3BP were expressed in *E. coli* and assayed. (H) Binding analysis of UBE2G2 and LGALS3BP *in vitro* with GST pull-down assays. Fusion protein beads were used for pull-down and detected with anti-GST and anti-FLAG antibodies. (I, J) Mel270 (I) and Omm2.5 (J) cells were transfected with plasmids encoding

melanoma cell marker, and VE-cadherin as a dual marker for endothelial vessels and VM pseudo vessels[22]. The $CD34^{-}$/VE-$cadherin^{+}$/$S100B^{+}$ structures represented the VM channel, and the ratio between VE-cadherin and CD34 staining represented the overall presence of VM. Interestingly, the VE-cadherin/CD34 ratio decreased in the UBE2G2-overexpressed group and increased in the silenced group (Fig. 3H and I, Fig. S3H and S3I). Similarly, Kaplan−Meier curves indicate that UBE2G2 overexpression significantly extended mice's lifespan, while UBE2G2 exerted the opposite effect (Fig. 3J and Fig. S3J).

These data illustrated that UBE2G2 suppresses UM cell metastasis and tube formation both *in vitro* and *in vivo*.

3.3. *UBE2G2 interacts with LGALS3BP and negatively regulates its protein level*

To further uncover the specific target of UBE2G2 responsible for its enzyme-independent function in UM progression, we performed label-free proteomic analysis and Co-immunoprecipitation coupled with mass spectrometry (Co-IP/MS) analyses in the MUM2B cell line (Fig. 4A). The label-free proteomic analysis detected a total of 118 upregulated and 191 downregulated proteins in the UBE2G2-upregulated group compared with the corresponding control cells (FC $\geq$ 1.2 or FC $\leq$ 0.83, P value $<$ 0.05; Fig. 4B, Supporting Information Table S4). Silver staining assay showed that the UBE2G2 immunoprecipitated group was observed with several specific bands of proteins compared to the IgG group. The differential proteins identified by Co-IP/MS were listed in Supporting Information Table S5 (Fig. 4C). We then integrated the UBE2G2-interacting proteins obtained from the Co-IP/MS experiment and the downregulated proteins revealed by proteomics analysis. We identified LGALS3BP as the protein that interacts with and is regulated by UBE2G2 (Fig. 4D and Supporting Information Fig. S4A). Immunofluorescent staining showed that LGALS3BP was more highly expressed in UM tissues than in normal tissues, contrary to the characteristics of UBE2G2 (Fig. S4B). Similarly, according to the Human Protein Atlas, LGALS3BP protein levels were high or medium in malignant melanoma but low in normal melanocytes (Fig. S4C). Kaplan−Meier plot revealed that patients with high LGALS3BP expression exhibited reduced distant metastasis-free survival based on the two databases (GSE22138 and GSE27831), as well as overall survival based on TCGA (Fig. S4D). Next, Co-IP experiments were employed to verify the physical binding between UBE2G2 and LGALS3BP. Results confirmed that endogenous UBE2G2 and LGALS3BP are associated with each other in UM cells, and hypoxia had no influence on their interaction (Fig. 4E and Fig. S4E). Then, we investigated exogenous interaction by overexpressing Flag-tagged UBE2G2 and Myc-tagged LGALS3BP in 293T cells (Fig. 4F). The interaction between UBE2G2 and LGALS3BP was also observed in GST pull-down assays and confirmed by Western blot analysis of the pull-down (Fig. 4G and H). In our proteomics results and eye tumor section staining, we found a negative correlation between the protein levels of LGALS3BP and UBE2G2. Per these, we speculated that the UBE2G2 might downregulate LGALS3BP. As expected, there appears to be a negative correlation and a dose-dependent relationship between LGALS3BP and UBE2G2 (Fig. 4I and J). Consistent with this idea, hypoxia inhibited the expression of UBE2G2 and subsequently upregulated endogenous LGALS3BP expression (Fig. 4K). On the other hand, ectopic expression of UBE2G2 significantly reduced the LGALS3BP protein levels increased by hypoxia (Fig. 4L). However, changing the oxygen concentration or manipulating UBE2G2 expression exogenously did not affect *LGALS3BP* mRNA levels, indicating that UBE2G2 regulates LGALS3BP stability through posttranscriptional mechanisms (Fig. S4F and S4G). These results demonstrated that UBE2G2 interacts with LGALS3BP and regulates its protein levels.

3.4. *UBE2G2 downregulates LGALS3BP by promoting ubiquitination degradation via residue*

It is unclear to which post-translational modifications participated in UBE2G2 regulating the stability of LGALS3BP. Thus, we next treated cells with CHX, a protein synthesis inhibitor, and monitored LGALS3BP expression. Results showed that the protein expression of LGALS3BP was increased in the presence of CHX, especially in UBE2G2-knockdown cells (Fig. 5A and B and Supporting Information Fig. S5A and S5B). In addition, the proteasome inhibitor MG132 reversed the decrease in LGALS3BP levels induced by UBE2G2 overexpression, suggesting that UBE2G2 regulates LGALS3BP stability through proteasome-mediated mechanisms (Fig. 5C). We thus speculated that UBE2G2 might degrade the stability of LGALS3BP utilizing ubiquitination. As depicted in Fig. 5D, the *in vitro* ubiquitination assay supported the hypothesis that UBE2G2 induces ubiquitination (Fig. S5C). In agreement, the ubiquitination of LGALS3BP was increased by the upregulation of UBE2G2 but decreased by the downregulation of UBE2G2 and hypoxia (Fig. 5E, Fig. S5D). However, it was not affected solely by hypoxia (Fig. S5E). To further gain insight into the ubiquitination sites of LGALS3BP essential for UBE2G2-mediated ubiquitination, we tested the effect of four domains separately on the ubiquitination of LGALS3BP. The molecular mapping revealed that the C-terminal domain (Del1: residues 1−125) was essential for the ubiquitination of LGALS3BP (Fig. 5F and G, Fig. S5F). Considering ubiquitin-modified lysine residues are highly conserved across eukaryotes, we subsequently generated lysine (K) to arginine (R) mutants of LGALS3BP (K104R and K110R) to verify our speculation. Significantly abolished ubiquitination was observed in the absence of LGALS3BP-K104R, indicating that LGALS3BP-K104R was the primary site for ubiquitination by UBE2G2 (Fig. 5H). Next, we investigated whether these mutations affect the degradation of LGALS3BP and found that only mutations of K104R abolished the degradation of LGALS3BP induced by UBE2G2 (Fig. S5G). In agreement with these findings, the mutant form of LGALS3BP K104R has a longer half-life compared to the WT form (Fig. 5I and Fig. S5H). These data suggested that UBE2G2 promotes the degradation of LGALS3BP by inducing its polyubiquitination at K104. Our next goal was to gain insight into the mechanism by

Myc-tagged LGALS3BP and the indicated amounts of Flag-tagged UBE2G2 for 24 h. Cell lysates were analyzed by Western blot with indicated antibodies. (K, L) UM cells with knockdown (K) or ectopic (L) expression of UBE2G2 cultured under normoxia and hypoxia were collected and then subjected to Western blotting. All data are presented as the mean ± SD of independent experiments.

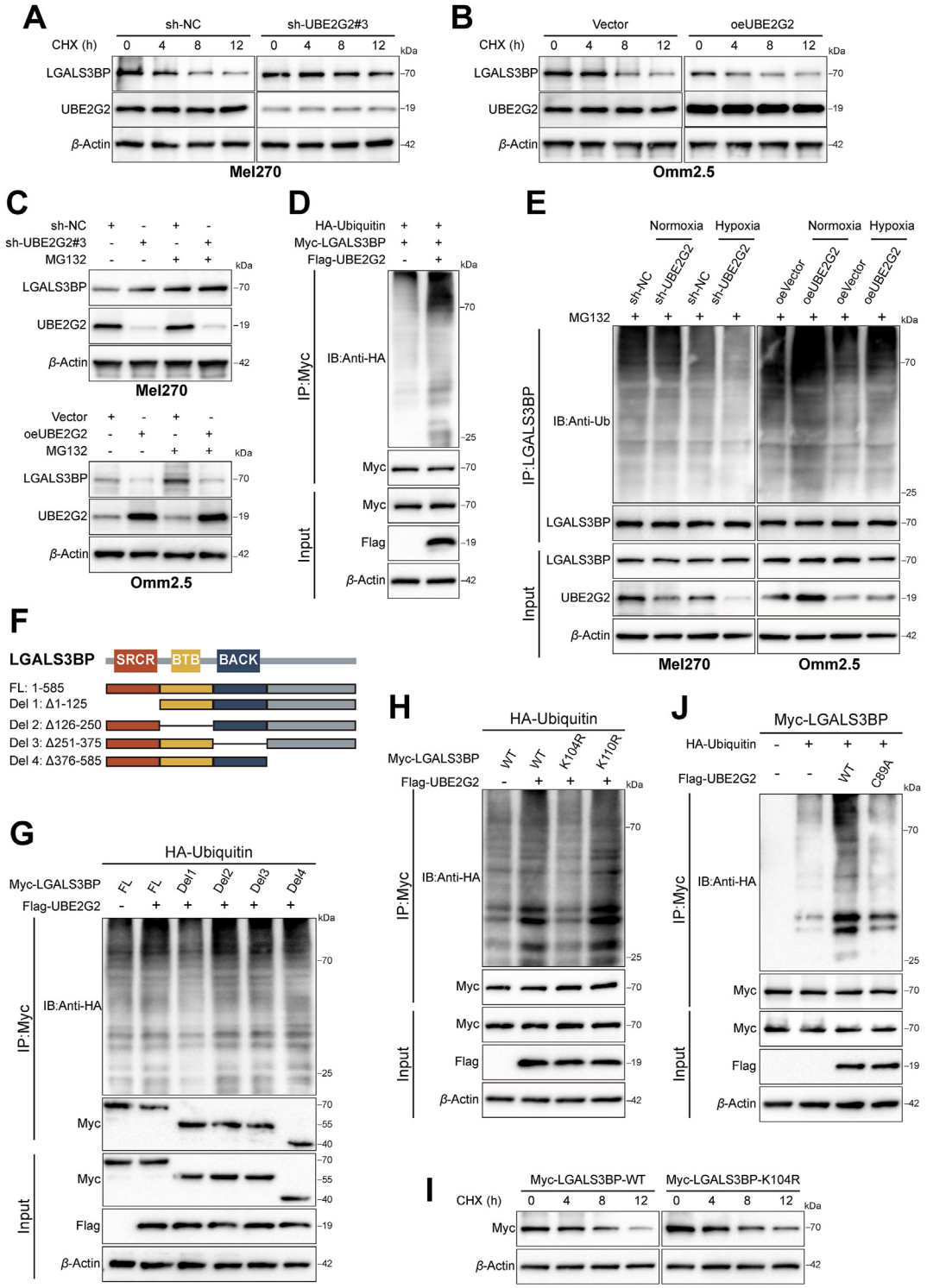

Figure 5 UBE2G2 promotes the polyubiquitination and degradation of LGALS3BP at K104 residue. (A, B) LGALS3BP expression levels in UM cells treated with cycloheximide (CHX) for the indicated times. (C) LGALS3BP protein levels in UBE2G2-knockdown or UBE2G2-overexpression UM cells treated with or without MG132. (D) HEK-293T cells were transiently transfected with plasmids expressing LGALS3BP and UBE2G2, along with HA-tagged ubiquitin. Ubiquitination of LGALS3BP in HA-tagged ubiquitin transfected cells. (E) UM cells were transfected with knockdown or ectopic UBE2G2 and cultured under normoxia and hypoxia. Cell lysates were analyzed by immunoblotting with indicated antibodies. (F) The schematic diagram of LGALS3BP truncations. (G) HEK-293T cells were transiently transfected with plasmids expressing Myc-tagged the deletion of the indicated domain of LGALS3BP and HA-tagged ubiquitin, along with plasmid expressing UBE2G2. Cell lysates were analyzed by immunoblotting with indicated antibodies. (H) HEK-293T cells were transiently transfected with plasmids expressing Myc-tagged indicated LGALS3BP mutant plasmids and HA-tagged ubiquitin plasmids, along with plasmid expressing UBE2G2. Cell lysates were analyzed by immunoblotting with indicated antibodies. (I) HEK-293T cells were transfected with Myc-LGALS3BP-WT or

which UBE2G2 facilitates the ubiquitination and subsequent degradation of LGALS3BP. Since the catalytic cysteine 89 (C89) residue is necessary to form UBE2G2-linked ubiquitin chains[24], we analyzed the poly-ubiquitination of LGALS3BP using UBE2G2 C89A mutant. The results showed that ubiquitination of LGALS3BP induced by ectopic UBE2G2 was significantly abolished upon UBE2G2 C89A mutant (Fig. 5J). Meanwhile, the UBE2G2 C89A mutant possessed an extended half-life of LGALS3BP compared to the WT form (Fig. S5I). Our data verified that UBE2G2 promotes K48-linked poly-ubiquitination of LGALS3BP but not K63-linked poly-ubiquitination (Fig. S5J). These findings confirm that UBE2G2 induces the poly-ubiquitination of LGALS3BP at K104 residue, leading to its degradation.

3.5. *UBE2G2 cooperates with ubiquitin E3 ligase TRIM38 to enhance the ubiquitination of LGALS3BP and inactivates the PI3K/AKT signaling pathway*

As the E2 targeting substrate for ubiquitination and degradation relies heavily on an E3 ligase, we speculated that an E3 ligase mediates UBE2G2-regulated LGALS3BP expression. After analyzing the mass spectrometry data, we identified tripartite motif containing 38 (TRIM38), an E3 ligase with a high abundance of UBE2G2-binding proteins (Supporting Information Fig. S6A). Based on published reports, TRIM38 acts as a link between E2s and substrates[25,26]. Endogenous and exogenous Co-IP experiments showed that UBE2G2 and TRIM38 were reciprocally immunoprecipitated (Fig. 6A and B). Moreover, overexpression of UBE2G2 and TRIM38 together led to a more significant promotion of LGALS3BP degradation and poly-ubiquitination than their individual ectopic expression (Fig. 6C and D, Fig. S6B). In contrast, knockdown TRIM38 significantly diminished the degradation of LGALS3BP and poly-ubiquitination induced by UBE2G2 (Fig. 6E and F). These results suggest that UBE2G2 promotes TRIM38-mediated ubiquitination and degradation of LGALS3BP, leading to down-regulation of LGALS3BP. In addition, LGALS3BP was reported to stimulate AKT, ERK and JNK signaling in melanoma[27−29]. Thus, we asked whether LGLAS3BP could induce these pathways to promote cancer metastasis and vascular mimicry in UM. When LGALS3BP was overexpressed in Omm2.5 cells, there was an increase in P-AKT, but no effect on P-ERK1/2, and a slight increase in P-JNK was observed. The opposite was observed as well (Fig. 6G and Fig. S6C). Next, we inquired if TRIM38 could enhance the potency of UBE2G2 in reducing LGALS3BP expression and inhibiting the PI3K/AKT signaling pathway. Depletion of UBE2G2 alone did not activate the PI3K/AKT signaling pathway as much as the simultaneous knockdown of TRIM38 and UBE2G2. However, these effects were reversed with LGALS3BP knockdown (Fig. 6H). Oppositely, The TRIM38 and UBE2G2 overexpression groups exhibited contrasting outcomes (Fig. 6I). Therefore, we confirmed that TRIM38 works together with UBE2G2, creating an E2−E3 duo that leads to the ubiquitination and degradation of LGALS3BP, suppressing the PI3K/AKT signaling pathway.

3.6. *UBE2G2 regulates the generation of an SPP1$^+$ macrophage population through UBE2G2−LGALS3BP axis*

As mentioned above, our results found that UBE2G2 induces the ubiquitination and degradation of LGALS3BP in UM cells in the presence of TRIM38. LGALS3BP is a secreted protein reported to modulate cell communication and immune responses. Therefore, we hypothesized that the UBE2G2−LGALS3BP axis influences the surrounding microenvironment to promote tumor progression and metastasis. To gain valuable insights into the potential role of the UBE2G2 in the cellular compartments involved in UM, we conducted single-cell transcriptomics on orthotopic tumors established by C57BL/6 mice (Fig. 7A and B). Major cellar compartments were identified based on known markers (Fig. 7C; Supporting Information Fig. S7A). LGALS3, the ligand of LGALS3BP, was upregulated in tumor-associated macrophages (TAMs) from oeUBE2G2 tumors (Fig. 7D and Fig. S7B). Results of qPCR analysis further established the *Lgals3* mRNA upregulation in TAMs after UBE2G2-overexpressing UM cell injection, and the downregulation in TAMs after injection of UBE2G2-depleted UM cells (Fig. 7E and Fig. S7C). Immunostaining showed that macrophages in the orthotopic tumors of the UBE2G2 overexpressed group expressed a high level of LGALS3 compared to the negative controls (Fig. 7F and Fig. S7D). Research has highlighted the significance of LGALS3 in facilitating macrophage migration and activation[30−32]. We then assessed the correlation between LGALS3 expression and gene signatures of M1/M2-like macrophages. The UM TCGA database showed a more significant positive correlation between *LGALS3* mRNA expression and M1-like macrophages (Fig. S7E).

Next, we isolated the macrophages in silico and identified 4 distinct subpopulations (clusters 2, 12, 18, 21; Fig. 7G). We observed a decrease in macrophage clusters 12 and 21 and an increase in clusters 2 and 18 in the tumor of the UBE2G2 overexpressed group (Fig. 7G and H). In cluster 12, the top four biomarkers were *Spp1*, *Ctsd*, *Cpnmb*, and *Apoe* (Fig. 7I). *SPP1*, which encodes osteopontin, is a prognostic and metastasis marker for melanoma[33−36]. Upon injection of UBE2G2 overexpressed UM cells, macrophages showed a suppressed expression of *Spp1* mRNA, while the injection of UBE2G2 deletion UM cells promoted the upregulation of *Spp1* in macrophages (Fig. 7J and Fig. S7F). Previous research has demonstrated that SPP1 has the ability to increase collagen expression in fibroblasts, which can lead to the promotion of fibrosis[37−40]. Consistent with prior literature, the oeUBE2G2 group with fewer SPP1$^+$ macrophages demonstrated a significant decrease in the proportion of fibroblasts (Fig. 7C). After re-clustering the fibroblasts, we observed a switch in the populations of fibroblasts, where cluster 7 was the major subpopulation in the control group, while cluster 15 became the predominant subpopulation in the UBE2G2-overexpressed group (Fig. 7K and L). Cluster 7 exhibited a collagen phenotype with *Col1a2* and *Ccn2* as top gene biomarkers (Fig. S7G and S7H). The transplantation of UM cells that overexpressed UBE2G2 resulted in the suppression of mRNA expression of CAF markers in fibroblasts and vice versa (Fig. 7M and Fig. S7I), which also led to an increase in fibrosis, as demonstrated by Masson trichrome staining (Fig. 7N). Instead, the deletion of UBE2G2 provoked

Myc-LGALS3BP-K104R plasmid and then treated with CHX for the indicated times before harvesting. Cell lysates were analyzed by immunoblotting with indicated antibodies. (J) HEK-293T cells were transfected with UBE2G2-WT or UBE2G2-C89A plasmid and HA-tagged ubiquitin plasmids, along with plasmids expressing Myc-tagged LGALS3BP. Cell lysates were analyzed by immunoblotting with indicated antibodies. All data are presented as the mean ± SD of three independent experiments.

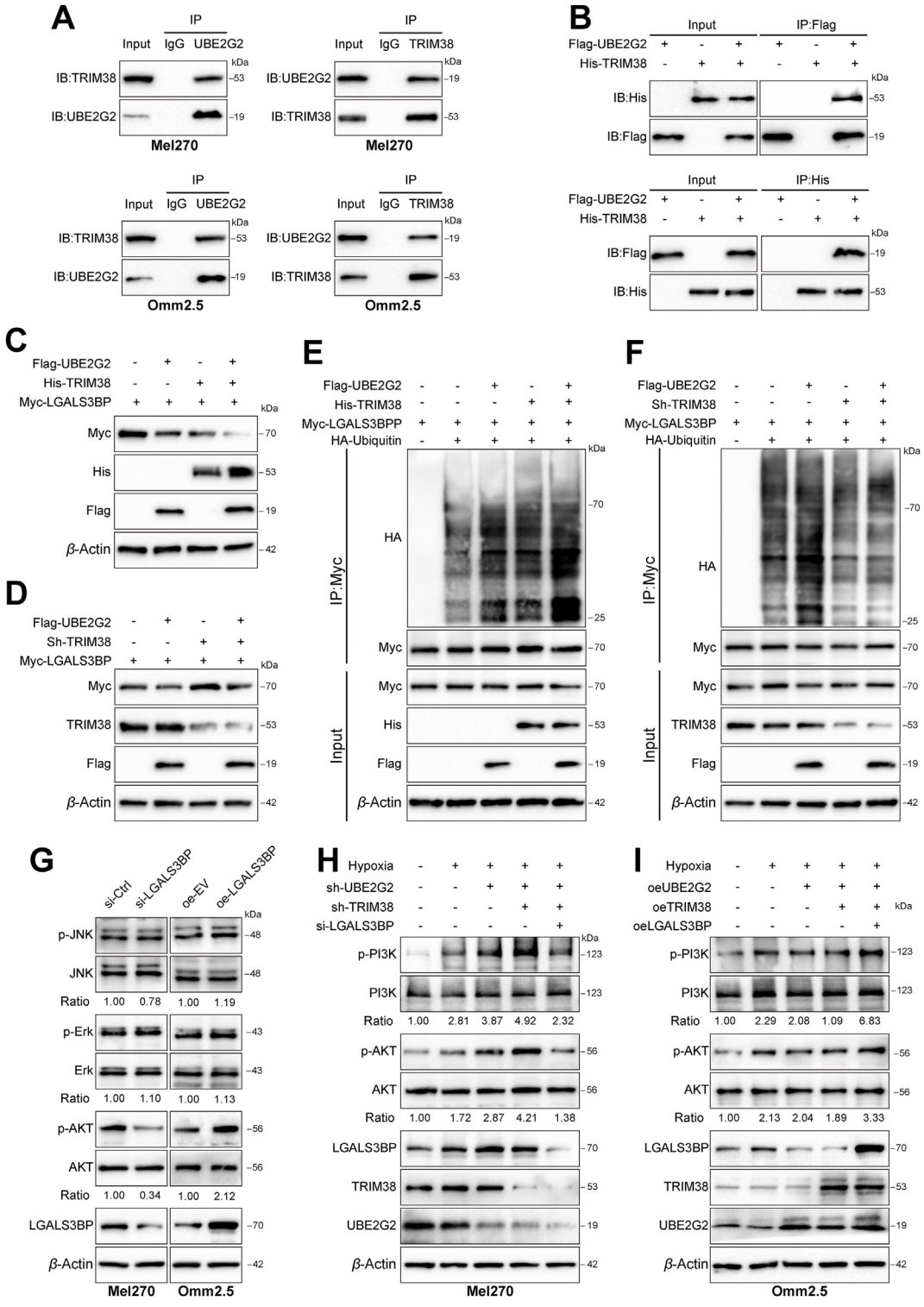

Figure 6 TRIM38 cooperates with UBE2G2 to enhance the poly-ubiquitination and degradation of LGALS3BP and suppress the PI3K/AKT signaling pathway. (A) Co-IP and Western blotting assay in Mel270 and Omm2.5 cells tested the endogenous interaction of UBE2G2 and TRIM38. (B) HEK-293T cells were transfected with indicated plasmids, and Co-IP and Western blotting assay detected the exogenous interaction between UBE2G2 and TRIM38. (C, D) Western blotting assay was used to detect the effect of TRIM38 cooperating with UBE2G2 on regulating LGALS3BP expression. (E, F) The effect of TRIM38 cooperating with UBE2G2 on poly-ubiquitination of RPS3. HEK-293T cells expressing the indicated plasmids were treated with MG132 (10 μmol/L) for 6 h. Cell lysates were immunoprecipitated with an anti-Myc antibody, followed by immunoblotting against indicated antibodies. (G) After transfected with knockdown or ectopic LGALS3BP, the protein levels of p-PI3K, PI3K, p-Erk, Erk, p-AKT, AKT, LGALS3BP and β-actin in UM cells were measured by Western blot analysis. (H, I) After transfected with knockdown (H) or ectopic (I) lentiviruses of UBE2G2, TRIM38 and LGALS3BP, the protein levels of p-PI3K, PI3K, p-AKT and AKT in UM cells were measured by Western blot analysis. All data are presented as the mean ± SD of three independent experiments.

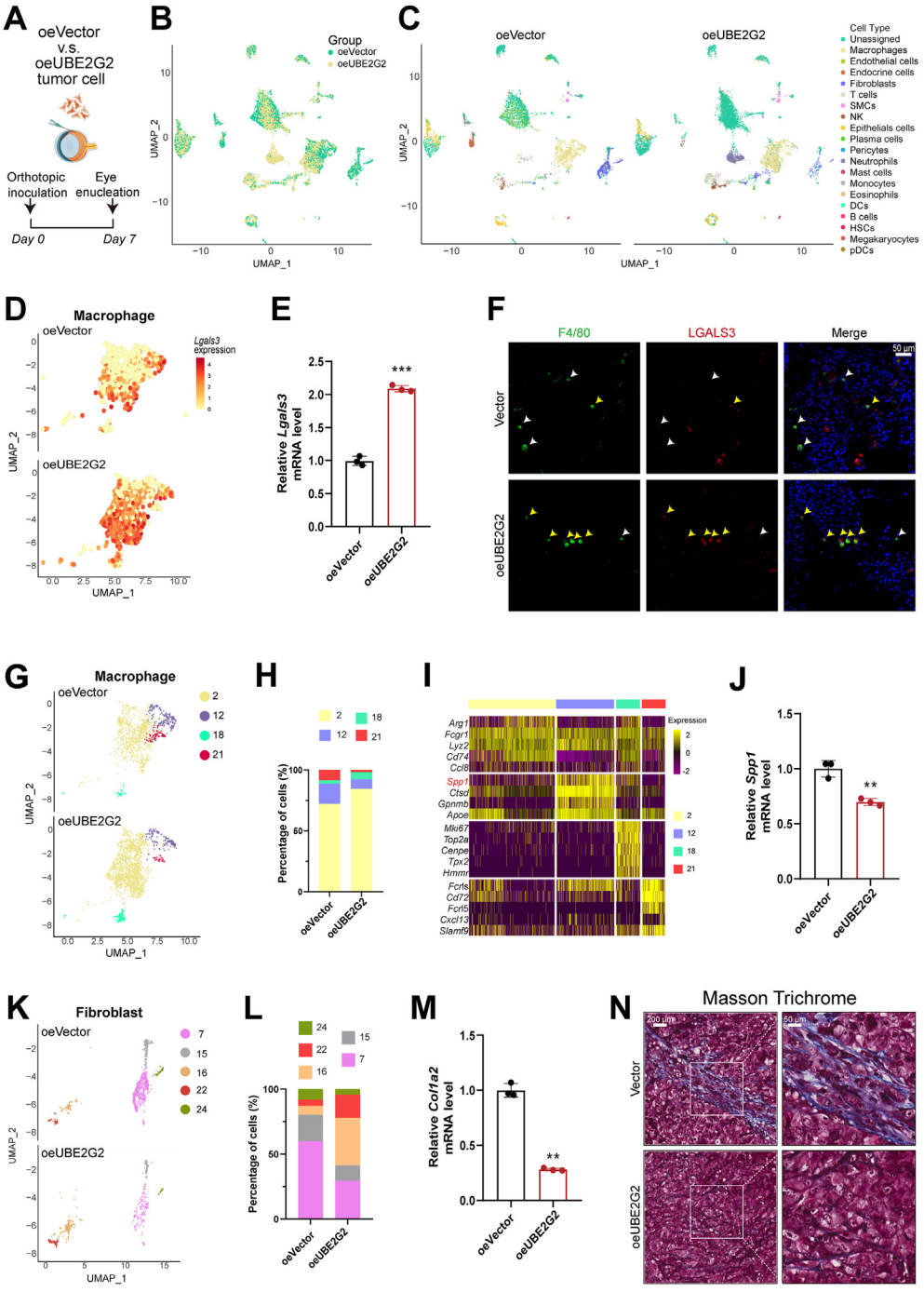

Figure 7 scRNA-Seq identifies UBE2G2-induced transcriptional signature in macrophages and fibroblasts. (A) Experimental design of orthotopic inoculation for scRNA-Seq. (B, C) Uniform Manifold Approximation and Projection (UMAP) plot with clustering results colored by sample (B) and by the major cellular compartments (C). (D, E) The distribution (D) and relative expression (E) of *Lgals3bp* in macrophages of the indicated groups. (F) Representative IF image showing F4/80 (a marker of macrophage) and LGALS3 staining in sections from orthotopic tumors from indicated groups. yellow arrow: LGALS3^{+}; white arrow: LGALS3^{-}. (G) UMAP plot with reclustering of macrophages, split by sample. (H) Stacked bar plots show the percentage of macrophages in each cluster. (I) Heatmap of the top-5 genes for each cluster. (J) The relative expression of *Spp1* in macrophages of the indicated groups. (K) UMAP plot with reclustering of fibroblasts, split by sample. (L) Stacked bar plots showing the percentage of fibroblasts in each cluster. (M) The relative expression of Col1a2 in fibroblasts of the indicated groups. (N) Masson trichrome staining in sections from orthotopic tumors from indicated groups. All data are presented as the mean ± SD of three independent experiments. $^{*}P < 0.05$, $^{**}P < 0.01$, $^{***}P < 0.001$.

opposite results (Fig. S7J). These data confirm that the UBE2G2−LGALS3BP axis also affected the composition of the extracellular matrix (ECM) in the context of uveal melanoma invasion.

3.7. *UBE2G2 suppresses tumor progression by improving the immunosuppressed microenvironment*

Emerging evidence suggests that the tumor microenvironment (TME) plays a crucial role in vasculogenic mimicry and tumor metastasis[41−43]. The high quantity of stromal components in the TME poses a significant challenge for immune effector cells to infiltrate the tumor tissue, ultimately forming an immunosuppressive microenvironment and promoting metastatic progression[44,45]. Thus, we observed changes in the proportions by using known markers to classify the scRNA-seq data into three primary cellular compartments. The results showed decreased stroma cells and increased immune cells in the UBE2G2 overexpressed group (Fig. 8A). However, no alterations were observed in the proportions of the epithelial compartment or its subpopulations

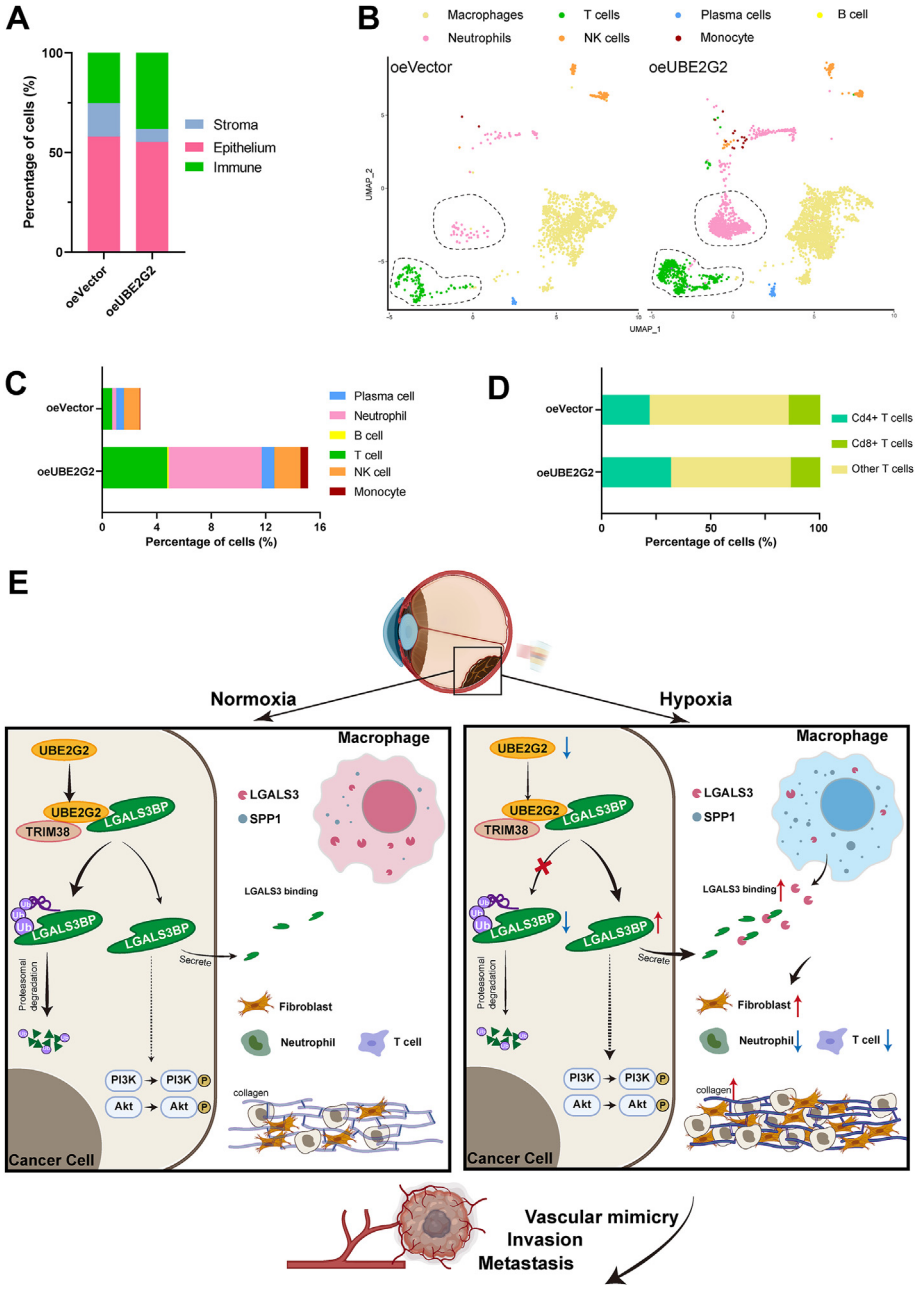

Figure 8 UBE2G2 reprograms the immune microenvironment *in vivo*. (A) Stacked bar plots showing the percentage of major cellular compartments. (B) UMAP plot of the immune compartment from orthotopic tumors. (C) The stacked bar plot illustrates the percentage of total cells occupied by immune cell types described in (B), except macrophages. (D) The stacked bar chart displays the percentage of total T cells occupied by $CD4^+$ T cells, $CD8^+$ T cells, and other subtypes. (E) The schematic indicates that UBE2G2 binds with LGALS3BP and TRIM38 to form a protein-binding complex that induces the ubiquitination and degradation of LAGLS3BP. This complex modulates the reprogramming of the tumor microenvironment against tumor progression, which is negatively regulated by hypoxia.

between two groups (Supporting Information Fig. S8A and S8B). As described above, the significant drop in fibroblastic cell count is the primary cause of the stromal reduction observed in the oeUBE2G2 group (Fig. 7K). Concomitant with the reduced content of fibroblasts, there was a consistent increase in the number of immune cells infiltrating in the oeUBE2G2 group, primarily attributed to the presence of neutrophils and T cells (Fig. 8B and C). Further analysis of the scRNA-seq data discovered that these tumors exhibited a shift in their neutrophil population, with cluster 5 being the predominant subpopulation in the UBE2G2 overexpressed tumor (Fig. S8C and S8D). The top biomarkers in cluster 5 were *S100a9* and *S100a8*, which agree with their dual effect in cancer (Fig. S8E). Specifically, a low concentration of S100A8/A9 has been shown to promote tumor growth, while a high concentration may have the opposite effect[46]. In agreement with the overexpression of UBE2G2 in tumors that exhibit a more immune-activated phenotype, an increased proportion of $CD8^+$ T cells was observed within these tumors (Fig. 8D). These findings suggest that overexpression of UBE2G2 can trigger a robust antitumor immune response and improve the tumor microenvironment in tumor-bearing mice. Collectively, all these data support that UBE2G2 acts as a crucial inhibitor in the oncogenetic UBE2G2/TRIM38/LAGALS3BP axis to suppress high steady-state levels of UM cell vascular mimicry and metastasis under hypoxic conditions (Fig. 8E).

4. Discussion

Growing evidence indicates that the involvement of VM in UM underscores its crucial role in the disease's progression and clinical outcomes. Notably, UM cases exhibiting VM often correlate with heightened invasiveness and metastatic potential, indicating that VM is a potential mechanism for the acquisition of aggressive phenotypes. Understanding the molecular intricacies of VM in UM holds significant therapeutic implications, offering a promising avenue for targeted interventions to impede UM progression and enhance patient outcomes. While the mechanisms of VM remain incompletely understood, growing research on the tumor microenvironment implies an inherent connection between the initial hypoxic conditions in solid tumors and the occurrence of VM. Our results demonstrate the presence of VM in hypoxic microenvironments, suggesting its adaptive significance as a survival strategy for tumor cells. Therefore, we selected MUM2B cells as a hypoxia model *in vitro* due to their robust representation of VM and high invasiveness, followed by identifying functionally relevant genes for detailed molecular studies.

Transcriptional regulation, especially HIF1α-dependent transcriptional regulation, has long been recognized as canonical, favoring cell survival regulation in response to the hypoxic response. However, relatively little is known about the role of posttranscriptional modification under hypoxic conditions. Ubiquitination serves as a pivotal post-translational modification process, regulating protein stability. In this study, we first established the molecular mechanism for the UBE2G2-dependent ubiquitin modification in tumor progression induced by hypoxia. Previous reports have highlighted UBE2G2 as a human E2 enzyme critical in mediating the ubiquitination and subsequent degradation process[47]. However, limited research reported that UBE2G2, as a ubiquitin-conjugating enzyme, promotes the occurrence and progression of cancer. To date, only one documentation reveals that non-small cell lung cancer patients exhibiting elevated UBE2G2 expression are associated with a relatively poor prognosis[48]. Clinically, we observed a significant downregulation of UBE2G2 expression in hypoxic domains of UM. Furthermore, our findings indicate that UBE2G2 inhibits the formation of VM and metastasis in UM induced by tumor hypoxia. These findings suggest that UBE2G2 may function as a tumor suppressor protein, exerting constraints on UM development and progression.

Gaining a comprehensive understanding of the mechanisms through which UBE2G2 exerts tumor suppressor effects is imperative for devising viable treatment strategies to enhance the prognosis of patients with UM. The convergence of findings from proteomics and IP/MS analyses revealed that UBE2G2 negatively regulates LGALS3BP, a modulator of cell communication and immune responses. Several studies have documented that LGALS3BP plays a role in downregulating target proteins through ubiquitination-mediated proteasomal degradation[49–51]. However, there is limited knowledge of LGALS3BP functions as a ubiquitination substrate involved in biological processes. A recent study reported that LGALS3BP enhances the ubiquitination of TRAF6 and TRAF3 and serves as a specific ubiquitination substrate for TRAF6, producing interferon and pro-inflammatory responses[52]. In the present study, we identified a ubiquitin-conjugating enzyme, UBE2G2, as an interacting upstream protein of LGALS3BP. Furthermore, MS results suggest that TRIM38, a ubiquitin ligase, may interact with UBE2G2, thereby facilitating the ubiquitin-dependent proteasomal degradation of LGALS3BP. Subsequent experiments demonstrated that the primary form of ubiquitination mediated by the collaboration of TRIM38 with UBE2G2 on LGALS3BP appears to be K48-linked ubiquitination, as opposed to other ubiquitin linkages.

LGALS3BP, also known as MAC-2BP or 90K, is a glycoprotein and a ligand of galectin-3. Belonging to the scavenger receptor cysteine-rich domain family of proteins, LGALS3BP is a secreted glycoprotein found in both intracellular and extracellular compartments. It is widely distributed in various body fluids. In recent years, significant attention has been directed towards understanding the potential role of LGALS3BP in human cancer progression. Elevated LGALS3BP expression is associated with increased growth in oral squamous cell carcinoma through PI3K/AKT pathway activation, and it contributes to lung cancer metastasis by enhancing integrin-mediated adhesion[29,53]. In breast cancer, endometrial cancer and cutaneous melanoma, LGALS3BP promotes angiogenesis through the galectin-3-dependent stimulation of the PI3K/AKT pathway[27–29]. Moreover, in cases of oxygen-induced retinopathy, LGALS3BP plays a role in microglia-mediated angiogenesis by upregulating angiogenesis-related factors[54]. This study underscored the significance of LGALS3BP in UBE2G2-mediated vasculogenic mimicry and the progression of tumors associated with VM. Consistent with previous studies, increased LGALS3BP activated the PI3K/AKT signaling pathway to regulate downstream cellular biological functions.

Increasing lines of evidence indicate that ECM remodelling induced by hypoxia is crucial for cancer metastasis and the phenomenon of vasculogenic mimicry[11,55]. The ECM stands out as one of the most vital components in shaping the TME. As a secreted protein, LGALS3BP binds to LGALS3, thereby facilitating cell-cell adhesion through bridging between galectin molecules attached to ECM components[56]. Therefore, we assumed that when UBE2G2 induces ubiquitination degradation of LGALS3BP to inhibit VM formation, ECM remodelling and TME may be involved in this process. Using single-cell RNA sequencing, we identified the entire transcriptional profile of UM cells with overexpressed UBE2G2. The results revealed that macrophages derived from the overexpressed

UBE2G2 group exhibit an elevated transcript of LGALS3, which is the binding partner of LAGLS3BP. According to the immunofluorescence results, there was a noticeable elevation in LGALS3 expression accompanied by the accumulation of intracellular protein aggregates. These phenomena could be attributed, at least in part, to diminished LGALS3BP binding. The research findings suggests that both LGALS3BP and LGALS3 can regulate macrophage polarity[57−59], thereby providing mechanistic support for the hypothesis that hypoxia induces $SPP1^+$ macrophage. Further investigation is necessary to elucidate the mechanisms underlying UBE2G2−LGALS3BP modulation of the microenvironment, particularly its impact on the $SPP1^+$ macrophage population.

Our findings also demonstrated that the overexpression of UBE2G2 in cancer cells leads to a downregulation in generating an $SPP1^+$ TAM population, reportedly responsible for the enhanced malignancy[40]. Prior studies have shown that LGALS3BP and SPP1 possess the capability to enhance collagen expression in fibroblasts, potentially contributing to ECM remodelling[37,38,60]. Here, we observed that overexpressing UBE2G2 in UM cells led to ECM remodelling, characterized by a reduction in the proportion of fibroblasts and a promotion of a shift towards subpopulations that exhibit lower reactivity and are less enriched in collagen phenotype. Notably, a recent study reported that hypoxia in UM could induce extracellular collagen matrix formation[11]. Hence, our data might provide mechanistic support for the idea that hypoxia contributes to ECM remodelling by downregulating UBE2G2, subsequently promoting the level of LGALS3BP and SPP1 in UM. Furthermore, UBE2G2-overexpressed cancer cells contribute to inhibiting metastasis and VM within the tumor and enhance the generation of an immunosuppressive tumor microenvironment by activating the immune system. This alteration is marked by notable changes in immune cell populations, including an increased number of neutrophils and T cells. Moreover, the T cells undergo a shift towards a more immune-activated phenotype.

Admittedly, it is important to acknowledge certain limitations of our study. While we have provided valuable insights into the role of UBE2G2 in UM, focusing solely on ubiquitination-associated genes may overlook the contributions of other genes and pathways in tumor development. The mechanism responsible for the downregulation of UBE2G2 under hypoxic conditions remains unknown and requires further investigation.

5. Conclusions

In summary, we demonstrated that UBE2G2 expression is downregulated in the uveal melanoma and inhibits VM and metastasis phenotype both *in vitro* and *vivo*, accompanied by a decreased desmoplastic response. At the mechanistic level, the reduction of UBE2G2 induced by hypoxia inhibits the ubiquitination and degradation of LGALS3BP, leading to the reprogramming of macrophages and promoting a switch to an SPP1-positive population. Our data demonstrate that targeting both intercellular and intracellular molecular mechanisms of the hypoxia−UBE2G2−LGALS3BP axis may contribute to developing various therapeutic strategies for UM.

Acknowledgments

We express our appreciation to all the participants in this study, including both the patients and the experimental animals that made sacrifices for the advancement of science. We want to thank the Core Facility of Jiangsu Provincial People's Hospital for its help in detecting experimental samples. This work is supported by the National Natural Science Foundation of China (Nos. 82273159 and 82171838) and the Jiangsu Province's Science and Technology Project (No. BE2020722, China). The sponsor or funding organization had no role in the design or conduct of this research.

Author contributions

Andi Zhao: Writing − review & editing, Writing − original draft, Visualization, Software, Methodology, Investigation, Formal analysis, Data curation. Chenyu Zhou: Resources, Data curation. Jinjing Li: Resources, Methodology. Zijin Wang: Resources. Hui Zhu: Resources. Shiya Shen: Resources. Qing Shao: Resources. Qi Gong: Resources. Hu Liu: Writing − review & editing, Project administration, Funding acquisition, Conceptualization. Xuejuan Chen: Writing − review & editing, Project administration, Funding acquisition, Conceptualization.

Conflicts of interest

The authors declare no potential conflicts of interest.

Appendix A. Supporting information

Supporting information to this article can be found online at https://doi.org/10.1016/j.apsb.2024.09.005.

References

1. Carvajal RD, Sacco JJ, Jager MJ, Eschelman DJ, Olofsson Bagge R, Harbour JW, et al. Advances in the clinical management of uveal melanoma. *Nat Rev Clin Oncol* 2023;**20**:99−115.
2. Rantala ES, Hernberg MM, Piperno-Neumann S, Grossniklaus HE, Kivela TT. Metastatic uveal melanoma: the final frontier. *Prog Retin Eye Res* 2022;**90**:101041.
3. Bustamante P, Piquet L, Landreville S, Burnier JV. Uveal melanoma pathobiology: metastasis to the liver. *Semin Cancer Biol* 2021;**71**:65−85.
4. Gilkes DM, Semenza GL, Wirtz D. Hypoxia and the extracellular matrix: drivers of tumour metastasis. *Nat Rev Cancer* 2014;**14**:430−9.
5. Rankin EB, Giaccia AJ. Hypoxic control of metastasis. *Science* 2016;**352**:175−80.
6. Yu P, Han Y, Meng L, Tian Y, Jin Z, Luo J, et al. Exosomes derived from pulmonary metastatic sites enhance osteosarcoma lung metastasis by transferring the miR-194/215 cluster targeting MARCKS. *Acta Pharm Sin B* 2024;**14**:2039−56.
7. Maniotis AJ, Folberg R, Hess A, Seftor EA, Gardner LM, Pe'er J, et al. Vascular channel formation by human melanoma cells *in vivo* and *in vitro*: vasculogenic mimicry. *Am J Pathol* 1999;**155**:739−52.
8. Ellis LM, Fidler IJ. Finding the tumor copycat. Therapy fails, patients don't. *Nat Med* 2010;**16**:974−5.
9. Dong L, You S, Zhang Q, Osuka S, Devi NS, Kaluz S, et al. Arylsulfonamide 64B inhibits hypoxia/HIF-induced expression of c-Met and CXCR4 and reduces primary tumor growth and metastasis of uveal melanoma. *Clin Cancer Res* 2019;**25**:2206−18.
10. Jha J, Singh MK, Singh L, Pushker N, Lomi N, Meel R, et al. Association of TYRP1 with hypoxia and its correlation with patient outcome in uveal melanoma. *Clin Transl Oncol* 2021;**23**:1874−84.
11. Kaluz S, Zhang Q, Kuranaga Y, Yang H, Osuka S, Bhattacharya D, et al. Targeting HIF-activated collagen prolyl 4-hydroxylase expression disrupts collagen deposition and blocks primary and metastatic uveal melanoma growth. *Oncogene* 2021;**40**:5182−91.

12. Viñas-Castells R, Beltran M, Valls G, Gómez I, García JM, Montserrat-Sentís B, et al. The hypoxia-controlled FBXL14 ubiquitin ligase targets SNAIL1 for proteasome degradation. *J Biol Chem* 2010; **285**:3794−805.
13. Lin HH, Li X, Chen JL, Sun X, Cooper FN, Chen YR, et al. Identification of an AAA ATPase VPS4B-dependent pathway that modulates epidermal growth factor receptor abundance and signaling during hypoxia. *Mol Cel Biol* 2012;**32**:1124−38.
14. Sulkshane P, Ram J, Thakur A, Reis N, Kleifeld O, Glickman MH. Ubiquitination and receptor-mediated mitophagy converge to eliminate oxidation-damaged mitochondria during hypoxia. *Redox Biol* 2021;**45**:102047.
15. Swatek KN, Komander D. Ubiquitin modifications. *Cell Res* 2016;**26**: 399−422.
16. Dikic I, Schulman BA. An expanded lexicon for the ubiquitin code. *Nat Rev Mol Cel Biol* 2023;**24**:273−87.
17. Zhao CX, Zeng CM, Wang K, He QJ, Yang B, Zhou FF, et al. Ubiquitin−proteasome system-targeted therapy for uveal melanoma: what is the evidence?. *Acta Pharmacol Sin* 2021;**42**:179−88.
18. Jiang Y, Ni S, Xiao B, Jia L. Function, mechanism and drug discovery of ubiquitin and ubiquitin-like modification with multiomics profiling for cancer therapy. *Acta Pharm Sin B* 2023;**13**:4341−72.
19. Cheng C, Yao H, Li H, Liu J, Liu Z, Wu Y, et al. Blockade of the deubiquitinating enzyme USP48 degrades oncogenic HMGA2 and inhibits colorectal cancer invasion and metastasis. *Acta Pharm Sin B* 2024;**14**:1624−43.
20. Zhao A, Wang Z, Wang Y, Chen X. Prognostic values of Annexins and validation of the influence on cell proliferation, migration, and invasion in uveal melanoma. *Am J Transl Res* 2023;**15**:3131−51.
21. Draper J, Alexander J, Nair RM, Scullion N, Narayana RVL, Aughton K, et al. Using the chick embryo model to examine the effects of hypoxia pre-conditioning of uveal melanoma cells on tumor growth and metastasis. *Curr Eye Res* 2023;**48**:408−15.
22. Fernandez-Cortes M, Delgado-Bellido D, Bermudez-Jimenez E, Paramio JM, O'Valle F, Vinckier S, et al. PARP inhibition promotes endothelial-like traits in melanoma cells and modulates pericyte coverage dynamics during vasculogenic mimicry. *J Pathol* 2023;**259**:318−30.
23. Kalirai H, Damato BE, Coupland SE. Uveal melanoma cell lines contain stem-like cells that self-renew, produce differentiated progeny, and survive chemotherapy. *Invest Ophthalmol Vis Sci* 2011;**52**:8458−66.
24. Li W, Tu D, Brunger AT, Ye Y. A ubiquitin ligase transfers preformed polyubiquitin chains from a conjugating enzyme to a substrate. *Nature* 2007;**446**:333−7.
25. Wang X, He H, Rui W, Zhang N, Zhu Y, Xie X. TRIM38 triggers the uniquitination and degradation of glucose transporter type 1 (GLUT1) to restrict tumor progression in bladder cancer. *J Transl Med* 2021;**19**:508.
26. Hu MM, Shu HB. Multifaceted roles of TRIM38 in innate immune and inflammatory responses. *Cell Mol Immunol* 2017;**14**:331−8.
27. Song Y, Wang M, Tong H, Tan Y, Hu X, Wang K, et al. Plasma exosomes from endometrial cancer patients contain LGALS3BP to promote endometrial cancer progression. *Oncogene* 2021;**40**:633−46.
28. Traini S, Piccolo E, Tinari N, Rossi C, La Sorda R, Spinella F, et al. Inhibition of tumor growth and angiogenesis by SP-2, an anti-lectin, galactoside-binding soluble 3 binding protein (LGALS3BP) antibody. *Mol Cancer Ther* 2014;**13**:916−25.
29. Stampolidis P, Ullrich A, Iacobelli S. LGALS3BP, lectin galactoside-binding soluble 3 binding protein, promotes oncogenic cellular events impeded by antibody intervention. *Oncogene* 2015;**34**:39−52.
30. MacKinnon AC, Farnworth SL, Hodkinson PS, Henderson NC, Atkinson KM, Leffler H, et al. Regulation of alternative macrophage activation by galectin-3. *J Immunol* 2008;**180**:2650−8.
31. S H, H DK, Y L, A JR, K I, Y T, et al. Human galectin-3 is a novel chemoattractant for monocytes and macrophages. *J Immunol* 2000; **165**:2156−64.
32. Chen A, Jiang Y, Li Z, Wu L, Santiago U, Zou H, et al. Chitinase-3-like 1 protein complexes modulate macrophage-mediated immune suppression in glioblastoma. *J Clin Invest* 2021;**131**:147552.
33. Deng G, Zeng F, Su J, Zhao S, Hu R, Zhu W, et al. BET inhibitor suppresses melanoma progression *via* the noncanonical NF-κB/SPP1 pathway. *Theranostics* 2020;**10**:11428−43.
34. Kadkol SS, Lin AY, Barak V, Kalickman I, Leach L, Valyi-Nagy K, et al. Osteopontin expression and serum levels in metastatic uveal melanoma: a pilot study. *Invest Ophthalmol Vis Sci* 2006;**47**:802−6.
35. Souri Z, Wierenga APA, van Weeghel C, van der Velden PA, Kroes WGM, Luyten GPM, et al. Loss of BAP1 is associated with upregulation of the NFκB pathway and increased HLA class I expression in uveal melanoma. *Cancers* 2019;**11**:1102.
36. Kashani-Sabet M, Nosrati M, Miller 3rd JR, Sagebiel RW, Leong SPL, Lesniak A, et al. Prospective validation of molecular prognostic markers in cutaneous melanoma: a correlative analysis of E1690. *Clin Cancer Res* 2017;**23**:6888−92.
37. Han H, Ge X, Komakula SSB, Desert R, Das S, Song Z, et al. Macrophage-derived osteopontin (SPP1) protects from nonalcoholic steatohepatitis. *Gastroenterology* 2023;**165**:201−17.
38. Morse C, Tabib T, Sembrat J, Buschur KL, Bittar HT, Valenzi E, et al. Proliferating SPP1/MERTK-expressing macrophages in idiopathic pulmonary fibrosis. *Eur Respir J* 2019;**54**:1802441.
39. Hoeft K, Schaefer GJL, Kim H, Schumacher D, Bleckwehl T, Long Q, et al. Platelet-instructed SPP1^{+} macrophages drive myofibroblast activation in fibrosis in a CXCL4-dependent manner. *Cell Rep* 2023; **42**:112131.
40. Bill R, Wirapati P, Messemaker M, Roh W, Zitti B, Duval F, et al. CXCL9:SPP1 macrophage polarity identifies a network of cellular programs that control human cancers. *Science* 2023;**381**:515−24.
41. Wei X, Chen Y, Jiang X, Peng M, Liu Y, Mo Y, et al. Mechanisms of vasculogenic mimicry in hypoxic tumor microenvironments. *Mol Cancer* 2021;**20**:7.
42. Herrera-Vargas AK, Garcia-Rodriguez E, Olea-Flores M, Mendoza-Catalan MA, Flores-Alfaro E, Navarro-Tito N. Pro-angiogenic activity and vasculogenic mimicry in the tumor microenvironment by leptin in cancer. *Cytokine Growth Factor Rev* 2021;**62**:23−41.
43. Kuo CH, Wu YF, Chang BI, Hsu CK, Lai CH, Wu HL. Interference in melanoma CD248 function reduces vascular mimicry and metastasis. *J Biomed Sci* 2022;**29**:98.
44. Kasashima H, Duran A, Martinez-Ordoñez A, Nakanishi Y, Kinoshita H, Linares JF, et al. Stromal SOX2 upregulation promotes tumorigenesis through the generation of a SFRP1/2-expressing cancer-associated fibroblast population. *Dev Cell* 2021;**56**:95−110.
45. de Castro LL, Lopes-Pacheco M, Weiss DJ, Cruz FF, Rocco PRM. Current understanding of the immunosuppressive properties of mesenchymal stromal cells. *J Mol Med Berl* 2019;**97**:605−18.
46. Chen Y, Ouyang Y, Li Z, Wang X, Ma J. S100A8 and S100A9 in cancer. *Biochim Biophys Acta Rev Cancer* 2023;**1878**:188891.
47. Lan Y, van Leur SW, Fernando JA, Wong HH, Kampmann M, Siu L, et al. Viral subversion of selective autophagy is critical for biogenesis of virus replication organelles. *Nat Commun* 2023;**14**:2698.
48. Zhao X, Yongchun Z, Qian H, Sanhui G, Jie L, Hong Y, et al. Identification of a potential tumor suppressor gene, UBL3, in non-small cell lung cancer. *Cancer Biol Med* 2020;**17**:76−87.
49. Piccolo E, Tinari N, D'Addario D, Rossi C, Iacobelli V, La Sorda R, et al. Prognostic relevance of LGALS3BP in human colorectal carcinoma. *J Transl Med* 2015;**13**:248.
50. Lee JH, Bae JA, Lee JH, Seo YW, Kho DH, Sun EG, et al. Glycoprotein 90K, downregulated in advanced colorectal cancer tissues, interacts with CD9/CD82 and suppresses the Wnt/β-catenin signal *via* ISGylation of beta-catenin. *Gut* 2010;**59**:907−17.
51. Park SY, Yoon S, Sun EG, Zhou R, Bae JA, Seo YW, et al. Glycoprotein 90K promotes E-Cadherin degradation in a cell density-dependent manner *via* dissociation of E-cadherin-p120-catenin complex. *Int J Mol Sci* 2017;**18**:2601.
52. Xu G, Xia Z, Deng F, Liu L, Wang Q, Yu Y, et al. Inducible LGALS3BP/90K activates antiviral innate immune responses by targeting TRAF6 and TRAF3 complex. *PLoS Pathog* 2019;**15**: e1008002.

53. Zhang X, Ding H, Lu Z, Ding L, Song Y, Jing Y, et al. Increased LGALS3BP promotes proliferation and migration of oral squamous cell carcinoma *via* PI3K/AKT pathway. *Cell Signal* 2019;**63**:109359.
54. Zhao C, Liu Y, Meng J, Wang X, Liu X, Li W, et al. LGALS3BP in microglia promotes retinal angiogenesis through PI3K/AKT pathway during hypoxia. *Invest Ophthalmol Vis Sci* 2022;**63**:25.
55. Xu Y, Zhou W, Ji Y, Shen J, Zhu X, Yu H, et al. Elongator promotes the migration and invasion of hepatocellular carcinoma cell by the phosphorylation of AKT. *Int J Biol Sci* 2018;**14**:518−30.
56. Niu L, Geyer PE, Wewer Albrechtsen NJ, Gluud LL, Santos A, Doll S, et al. Plasma proteome profiling discovers novel proteins associated with non-alcoholic fatty liver disease. *Mol Syst Biol* 2019;**15**:e8793.
57. Shirakawa K, Endo J, Kataoka M, Katsumata Y, Yoshida N, Yamamoto T, et al. IL (Interleukin)-10−STAT3−galectin-3 axis is essential for osteopontin-producing reparative macrophage polarization after myocardial infarction. *Circulation* 2018;**138**:2021−35.
58. Wu Q, Sun S, Wei L, Liu M, Liu H, Liu T, et al. Twist1 regulates macrophage plasticity to promote renal fibrosis through galectin-3. *Cell Mol Life Sci* 2022;**79**:137.
59. Pei C, Zhang Y, Wang P, Zhang B, Fang L, Liu B, et al. Berberine alleviates oxidized low-density lipoprotein-induced macrophage activation by downregulating galectin-3 *via* the NF-κB and AMPK signaling pathways. *Phytother Res* 2019;**33**:294−308.
60. Capone E, Iacobelli S, Sala G. Role of galectin 3 binding protein in cancer progression: a potential novel therapeutic target. *J Transl Med* 2021;**19**:405.